Article

Cell Reports

Mesenchymal Cancer Cell-Stroma Crosstalk Promotes Niche Activation, Epithelial Reversion, and Metastatic Colonization

Graphical Abstract

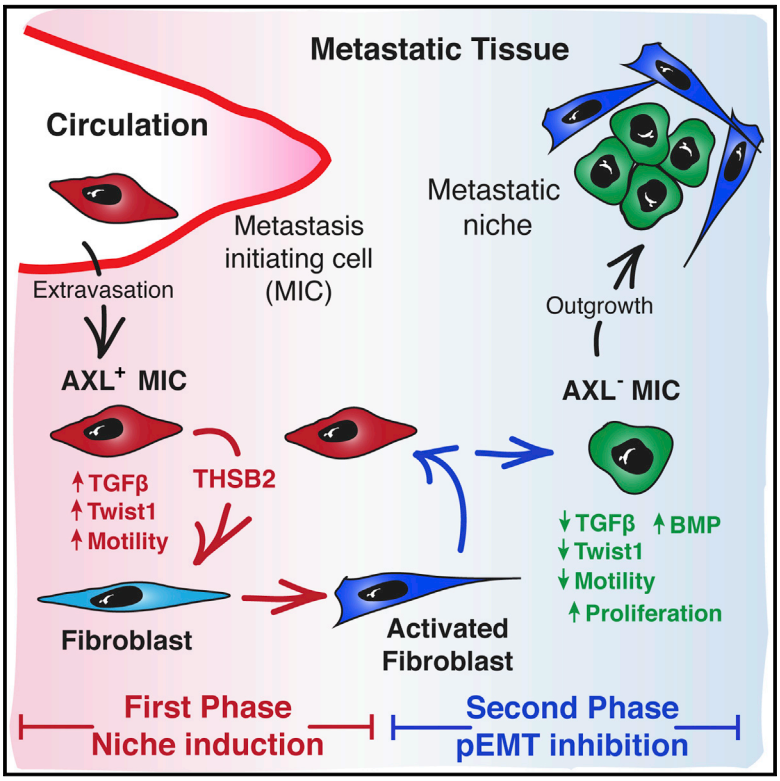

Authors

Yaiza del Pozo Martin, Danielle Park, Anassuya Ramachandran, ..., Caroline S. Hill, Erik Sahai, Ilaria Malanchi

Correspondence

ilaria.malanchi@crick.ac.uk

In Brief

del-Pozo-Martín et al. find that a mesenchymal state characterized by AXL expression triggers cancer cell-stromal cell crosstalk upon infiltration of the secondary site. These interactions affect metastatic colonization and, ultimately, lead cancer cell reversion to a more epithelial state.

Highlights

- AXL$^+$ mesenchymal-state cells have a higher capacity to activate fibroblasts
- AXL-EMT-dependent fibroblast activation is enhanced by THSB2
- Activated fibroblasts promote cancer cell plasticity toward a more epithelial state
- This epithelial shift is associated with a BMP-dependent growth

Accession Numbers

GSE63558

del Pozo Martin et al., 2015, Cell Reports *13*, 2456–2469
December 22, 2015
http://dx.doi.org/10.1016/j.celrep.2015.11.025

OPEN ACCESS
CellPress

Cell Reports
Article

Mesenchymal Cancer Cell-Stroma Crosstalk Promotes Niche Activation, Epithelial Reversion, and Metastatic Colonization

Yaiza del Pozo Martin,[1] Danielle Park,[2] Anassuya Ramachandran,[3] Luigi Ombrato,[1] Fernando Calvo,[6] Probir Chakravarty,[4] Bradley Spencer-Dene,[5] Stefanie Derzsi,[2] Caroline S. Hill,[3] Erik Sahai,[2] and Ilaria Malanchi[1,*]
[1]Tumor-Stroma Interactions in Cancer Development
[2]Cell Biology of the Tumor Microenvironment
[3]TGF-β Superfamily Signalling in Development and Cancer
[4]Bioinformatics and BioStatistics Team
[5]Experimental Histopathology Unit
The Crick Institute, Lincoln's Inn Fields Laboratory, 44 Lincoln's Inn Fields, WC2A 3LY London, UK
[6]Tumor Microenvironment Team, Division of Cancer Biology, The Institute of Cancer Research, 237 Fulham Road, SW3 6JB London, UK
*Correspondence: ilaria.malanchi@crick.ac.uk
http://dx.doi.org/10.1016/j.celrep.2015.11.025

SUMMARY

During metastatic colonization, tumor cells must establish a favorable microenvironment or niche that will sustain their growth. However, both the temporal and molecular details of this process remain poorly understood. Here, we found that metastatic initiating cells (MICs) exhibit a high capacity for lung fibroblast activation as a result of Thrombospondin 2 (THBS2) expression. Importantly, inhibiting the mesenchymal phenotype of MICs by blocking the epithelial-to-mesenchymal transition (EMT)-associated kinase AXL reduces THBS2 secretion, niche-activating ability, and, consequently, metastatic competence. Subsequently, disseminated metastatic cells revert to an AXL-negative, more epithelial phenotype to proliferate and decrease the phosphorylation levels of TGF-β-dependent SMAD2-3 in favor of BMP/SMAD1-5 signaling. Remarkably, newly activated fibroblasts promote this transition. In summary, our data reveal a crosstalk between cancer cells and their microenvironment whereby the EMT status initially triggers and then is regulated by niche activation during metastatic colonization.

INTRODUCTION

Solid epithelial tumors are complex structures in which associated stromal cells, including fibroblasts, support cancer cells. During metastatic progression, cancer cells disseminate from their tissue of origin to re-establish the tumor structure in distant organs. Efficient metastasis requires the expression of specific molecules, such as POSTN and TNC, within the local microenvironment (Malanchi et al., 2012; Oskarsson et al., 2011). Therefore, a favorable microenvironment, or niche, is a crucial early requirement for metastatic progression (Sleeman, 2012). However, the factors that promote efficient metastatic niche activation remain poorly characterized.

Cancer cells display heterogeneity in intrinsic tumorigenic potential; only a small subset of cells within tumors retains the ability of sustaining long-term growth (Hermann et al., 2007; Malanchi et al., 2008) as well as triggering relapses (Chen et al., 2012). Cancer cells with the stem cell-like property of self-renewal can be defined functionally as cancer-initiating cells (CICs) for their capacity to elicit tumor growth. Moreover, metastatic initiating cells (MICs) can be distinguished from the bulk of cancer cells for their ability to establish metastasis. The functional assay for MICs involves determining the extent to which single cells can grow in a foreign tissue and is more challenging than the equivalent orthotopic transplantation assay used to assess the ability of CICs to initiate tumor growth. Although self-renewal ability is a common requirement for the re-initiation of a cancer cell mass at either primary or secondary sites, additional characteristics that discriminate MICs from CICs have not been explored. MICs have been identified previously in the mouse breast cancer model where mouse mammary tumor virus promoter controls the expression of the polyomavirus middle T antigen (MMTV-PyMT) (Malanchi et al., 2012). We hypothesized that, in addition to intrinsic tumorigenic potential, MICs would exhibit a higher capacity for interacting with their niche by activating naive cells at distant sites (Malanchi, 2013).

One strategy adopted by carcinoma cells to disseminate from the primary tumor mass is the activation of the developmental program epithelial-to-mesenchymal transition (EMT). During EMT, epithelial cells undergo a global change in cell architecture, leading to the loss of cell-cell adhesions in favor of cell-extracellular matrix (ECM) interactions and cell migration (Thiery et al., 2009). Notably, EMT modulations are not binary, but a graded range of intermediate states exists. The process is initiated by the activation of the EMT core transcription factors (TFs) Snail, Zeb, and Twist1 (Peinado et al., 2007), which drive epithelial cancer cells to switch off the expression of epithelial markers such as the adherens junction protein E-Cadherin and activate the expression of mesenchymal markers such as Vimentin. The tyrosine kinase AXL is a downstream effector of the EMT program (Vuoriluoto et al.,

2011). EMT in breast cancer cells triggers an increase in AXL expression, and inhibition of AXL reduces the invasive and tumorigenic behavior of cancer cells (Gjerdrum et al., 2010; Holland et al., 2010; Sheridan, 2013; Paccez et al., 2014).

Interestingly, the induction of EMT TFs correlates with the emergence of stem cell-like properties (Mani et al., 2008; Morel et al., 2008). This suggests that the gain of mesenchymal characteristics might not only affect dissemination from primary tumors but also boost the stem cell properties required for metastatic outgrowth. However, epithelial characteristics are re-acquired at metastatic locations via mesenchymal-to-epithelial transitions (METs), typically leading to the establishment of secondary tumors with epithelial phenotypes (Tsai et al., 2012). The outgrowth of metastases requires cancer cell self-renewal and growth ability. Therefore, in the context of metastatic growth, "stemness" is not strictly coupled to the mesenchymal features of cancer cells. The potential advantage of a more mesenchymal state of cancer cells at the metastatic site and the origin of their epithelial plasticity remain unclear.

In this study, we use breast cancer models to demonstrate that the EMT program is a key regulator of the enhanced niche activation capacity of MICs at secondary sites. We identify Thrombospondin 2 (THBS2) as a mesenchymal state-dependent effector of cancer cells that promotes stromal niche activation. Subsequently, the newly activated stroma promotes cancer cells to shift toward a more epithelial, BMP-dependent state compatible with proliferation. We elucidated a biphasic temporal regulation during metastatic colonization whereby the mesenchymal status of cancer cells promotes stromal activation, which, in turn, promotes cancer cell epithelial plasticity and their reversion to a more epithelium-like phenotype.

RESULTS

MICs Display Partial EMT Features

In the mouse breast cancer MMTV-PyMT model, MICs were identified by co-expression of the CD24 and CD90 markers (Malanchi et al., 2012). The gene expression profile of MICs ($CD24^+CD90^+$) was compared to that of non-MICs ($CD24^+CD90^-$) to generate a MIC signature (Figure S1A). We verified that high levels of Wnt signaling are a hallmark of metastatic cancer stem cells (Malanchi et al., 2008, 2012; Nguyen et al., 2009; Reya and Clevers, 2005; Vermeulen et al., 2010), along with other characteristics associated with their high metastatic potential, such as active transforming growth factor β (TGF-β) signaling (Padua et al., 2008) and Yap/Taz activity (Diepenbruck et al., 2014). We also found that the MIC signature exhibited characteristic features of EMT and its related extracellular matrix remodeling (Figure 1A and S1B). In line with this, MICs freshly isolated from primary tumors displayed a mesenchymal phenotype with higher expression of Vimentin and the EMT-related receptor AXL as well as reduced E-cadherin levels (Figures 1B and 1C). This more mesenchymal phenotype was corroborated functionally using Matrigel collagen matrices where MICs, either in pure or mixed non-MIC/MIC spheroids, displayed enhanced single-cell invasive behavior compared with non-MICs (Figures 1D, 1E, and S1C).

The capacity of MICs for invasion correlated with increased expression levels of actin cytoskeleton regulators and extracellular matrix components (Figures S1D and S1E). EMT in MICs was further confirmed by the higher expression and nuclear localization of EMT TFs (Figures S1F and S1G). However, the high level of heterogeneity within the MIC population suggests a graded EMT with intermediate "partial EMT" states rather than a simple binary transition. The MIC expression signature also correlated with different secretome gene sets (Figure 1A). Some of these secreted factors have been reported previously to play a role in metastasis, such as TNC, SPARC, or CCL2 (Oskarsson et al., 2011, Tichet et al., 2015; Qian et al., 2011).

We went on to investigate the influence that the observed partial EMT status of MICs has on their capacity for metastatic initiation following dissemination. Because the metastatic behavior of MMTV-PyMT MICs might be regulated by the activity of other pathways, such as WNT (Figure 1A), we selected a broader mesenchymal cancer cell pool expressing AXL, including the MIC ($CD24^+CD90^+$) population (Figure S2A). As expected, the $CD24^+AXL^+$ population isolated from primary tumors displayed partial mesenchymal features (Figures S2B and S2C). We next tested $CD24^+AXL^+$ cells for their cancer initiation and metastatic initiation potential using orthotopic transplantation and tail vein injection, respectively (Figures 1F and 1G). Both assays require cancer cell stemness to reinitiate and sustain a cancer cell mass, either in a collective challenge within their organ of origin with favorable niches or when seeded via circulation as single cells in a likely less favorable "foreign" organ. We observed no difference in primary tumor growth for $CD24^+AXL^+$ and $CD24^+AXL^-$ cells, indicating that the subpools exhibit a comparable capacity for cancer initiation (Figure 1H). Indeed, for MMTV-PyMT tumor cells, more mesenchymal characteristics do not appear to influence tumor initiation ability. The more epithelial $CD24^+SCA1^+$ subpool (Figures S2D–S2F) identified previously for their tumor initiation capacity (Liu et al., 2007) displayed a similar tumor initiation potential as the more mesenchymal $CD24^+AXL^+$ or MIC pools (Figures S2G–S2I). Strikingly, $CD24^+AXL^+$ cancer cells show a higher lung metastasis competence compared with their more epithelial counterparts (Figure 1I). This suggests that the common mesenchymal characteristics observed within the $CD24^+AXL^+$ and MIC $CD24^+CD90^+$ cancer cells might be linked functionally to their metastatic competence, independent of an advantage in intrinsic stemness potential displayed in a favorable microenvironment.

MICs Promote Quicker Lung Fibroblast Activation

The highly secretory mesenchymal status of MICs might provide an increased capacity of generating a favorable environment, or niche, in distant sites (Figure 1A). We examined this suggestion by analyzing the activation of lung stromata around disseminated AXL^+ or AXL^- cancer cell early after their extravasation into the lungs. In line with our hypothesis, $CD24^+AXL^+$ cells are surrounded by higher numbers of smooth muscle actin (SMA)-activated fibroblastic stroma compared with $CD24^+AXL^-$ cells. We observed no difference in their tissue localization, in particular in their proximity to lung endothelial cells (Figures 2A–2D). To test whether niche activation ability is a common advantage conferred by the mesenchymal status of $CD24^+AXL^+$ and MIC pools, we measured the ability of isolated MICs to trigger features of cancer-associated fibroblasts (CAFs) in normal lung fibroblasts ex vivo. Sorted MICs or

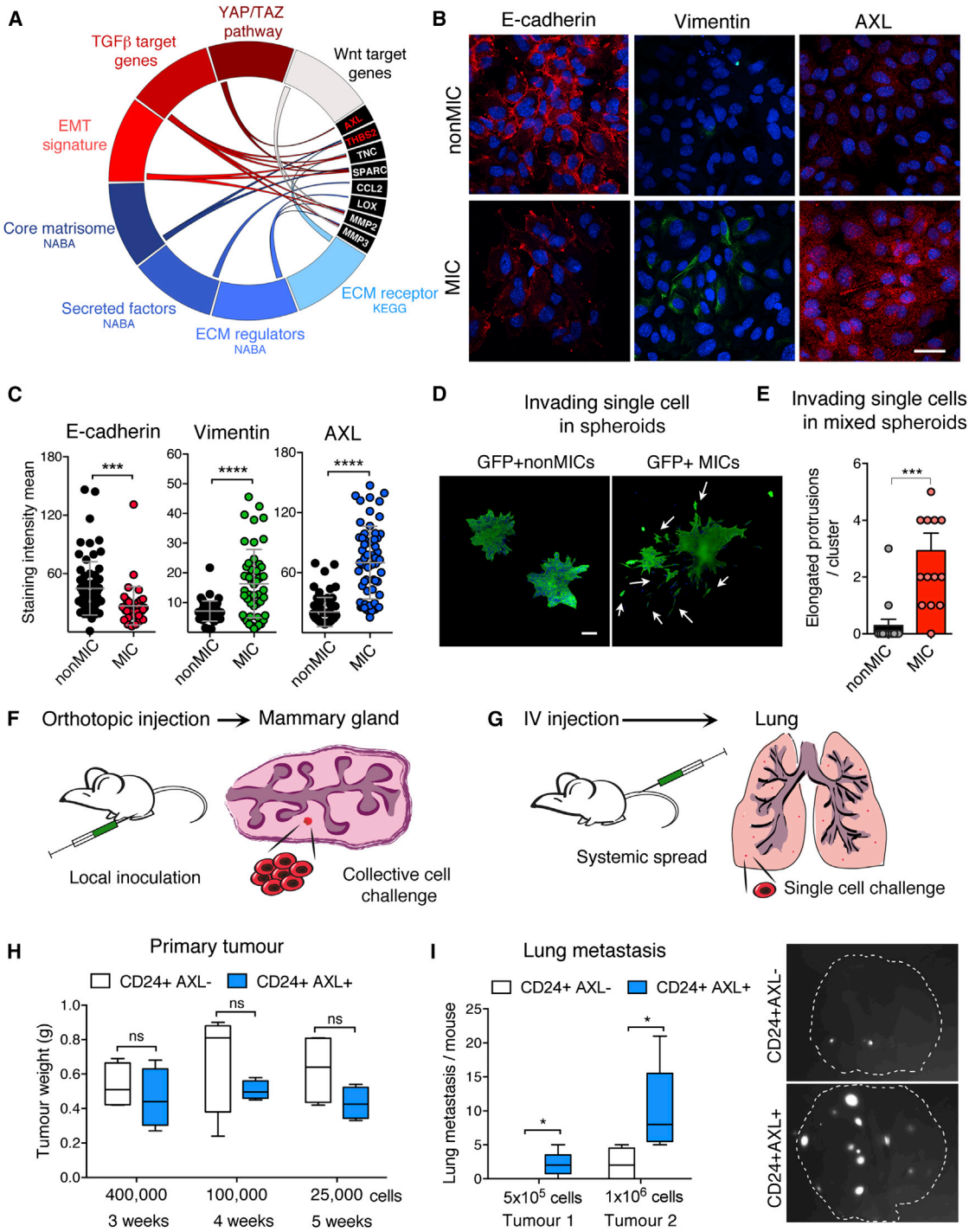

Figure 1. The Mesenchymal Features of MICs Are Part of Their Metastasis-Initiating Potential

(A) Circos plot displaying selected gene signatures correlating positively with MIC-upregulated genes (see also Figures S1A and S1B). Black blocks highlight metastasis-promoting genes either known (white) or described in this study (red).

(B and C) Representative immunofluorescence images (B) of non-MICs ($CD24^{+}CD90^{-}$) and MICs ($CD24^{+}CD90^{+}$) stained with E-cadherin, Vimentin, and AXL antibodies. Scale bar, 40 μm. Staining quantification is shown in (C). Data are from one representative experiment of five.

(D) Spheroid invasion assay. Shown are representative fluorescence images of MIC or non-MIC spheroids from actin-GFP/PyMT tumors in Matrigel:collagen I. Scale bar, 100 μm.

(E) Mixed spheroid invasion assay. The histogram shows the number of cells invading as single cell (1:9 actin/GFP MICs:non-labeled non-MICs) in Matrigel:collagen I (see also Figure S1C).

(legend continued on next page)

non-MICs with a GFP-labeled normal lung fibroblast cell line (NLF3) were plated and monitored for the induction of early fibroblast activation markers (Figure 2E). Because all cancer cells are capable of fibroblast activation to some extent, we used low cell numbers to increase the assay's sensitivity. After 24 hr, fibroblasts co-cultured with MICs exhibited early nuclear YAP translocation, required for CAF induction, and higher fibroblast activation protein (FAP) expression compared with fibroblasts cultured with non-MICs (Figures 2F–2H; Calvo et al., 2013). To verify that the induction of these markers represents fibroblast activation, we performed functional gel contraction assays to examine the ability of fibroblasts to physically remodel the ECM. Limited numbers of cell-sorted MICs or non-MICs from primary tumors were seeded in the upper chamber of a trans-well dish. In the lower chamber of the co-culture, normal lung fibroblasts (NFs) freshly isolated from wild-type mouse lungs were embedded in collagen-Matrigel matrices (Figure 2I). Importantly, we observed that MICs trigger significantly greater fibroblast-driven gel contraction compared with the other primary cancer cells (Figures 2J). In parallel, a gain of a CAF gene expression signature was induced in fibroblast co-cultured with MICs. Collectively, these data provide direct evidence that cancer cells displaying partial EMT characteristics show an enhanced ability to generate activated fibroblasts, a crucial component of the metastatic niche.

Thrombospondin 2 Secretion Increases Stromal Activation Capacity and Confers a Metastatic Advantage in MICs

To understand the mechanism underlying the enhanced capacity for fibroblast activation, we tested several MIC-specific secreted proteins for their ability to activate fibroblasts (Figures S3A and S3B). We found that purified recombinant THBS2 significantly enhanced the gel contraction capacity of fibroblasts (Figure 3A). We observed that exposure of lung fibroblasts to purified THBS2 led to activation of integrin β1 and the phosphorylation of its downstream effector focal adhesion kinase (pFAK) (Figures 3B and 3C). Importantly, a specific integrin β1-blocking antibody (β1BA) arrested the THBS2-dependent integrin cascade as well as fibroblast activation (Figures 3B–3D). To examine the role THBS2 might play in tumorigenicity, we used a specific short hairpin RNA (shRNA) targeting *Thbs2* mRNA (shTHBS2) to knock down its expression in primary MMTV-PyMT cancer cells (PyMT) (Figure 3E). Importantly, THBS2 depletion rendered cancer cells less able to activate lung fibroblasts (Figure 3F). Furthermore, shTHBS2 cancer cells were reduced dramatically in their capacity for lung metastatic colonization upon intravenous injection (Figure 3H). However, this is unlikely to be due to an effect on intrinsic cancer cell stemness because shTHSB2 PyMT cells maintained their ability to initiate early primary tumor growth in vivo or form spheres in vitro (Figure 3G and S3C). Similar findings were obtained using a second shRNA to block THBS2 secretion (Figures S3D–S3H). Because THBS2 is highly expressed in only a subset of PyMT cells, we tested the consequence of exogenous *Thbs2* gene expression in all PyMT cells. Importantly, broad THBS2 secretion resulted in increased early metastatic growth in the lungs upon direct seeding (Figure 3I). These data support the clinical correlation of high *Thbs2* expression with poor prognosis in advanced-stage human breast cancers (Figure S3I). Together, these results suggest that MICs mediate efficient fibroblast activation through THBS2 secretion and that this is critical for efficient metastatic initiation within the secondary tissue.

The Niche Activation Capacity of Metastatic Cancer Cells Depends on Their Partial Mesenchymal Status

The previous results reveal high niche activation ability as a crucial characteristic of MICs. Interestingly, we also found that their partial EMT phenotype defined by AXL expression was sufficient to determine their metastatic competence (Figure 1I). Therefore, we investigated whether the high niche activation ability of MICs is linked functionally to their AXL mesenchymal status. We used two approaches to downregulate AXL. First we used the AXL-specific small molecule inhibitor R428 (Holland et al., 2010), and second we used an shRNA to target *Axl* mRNA (Gjerdrum et al., 2010). Brief exposure of MICs to R428 triggered an overall shift toward a more epithelial phenotype with lower Vimentin and AXL expression and higher E-cadherin levels (Figures 4A, 4B, and S4A). Accordingly, we detected a reduction in the expression of EMT-TFs and motility in MICs (Figures S4B and S4C). Similar phenotypic changes occurred in the basal human breast cancer cell line MDA-MB-231 (MDA231) following treatment with R428. Indeed, although MDA231 cells, which homogeneously express AXL, typically display mesenchyme-like features, a single pulse of R428 reduced the expression of AXL and Vimentin and cell motility for up to 48 hr (Figures S4D–S4G). Interestingly, upon R428-mediated mesenchymal inhibition, cancer cells also reduced the expression of secreted factors, including THBS2 (Figures 4C and S4H). Concomitantly, the fibroblast activation ability of R428-treated metastatic cells was impaired dramatically (Figure 4D). Because similar results were found using an shRNA against *Axl* mRNA in primary PyMT cells (Figure S5A), we can exclude non-specific effects of the small molecule inhibitor R428. Indeed, shRNA-induced AXL downregulation in PyMT cells reduced THBS2 secretion and ex vivo fibroblast activation abilities (Figures 4E and 4F). Notably, the expression of *Thbs2* appears to be highly linked to the expression of the *Axl* and *Twist1* genes in human tumor biopsies (Figure S4I). These data demonstrate that the mesenchymal status of MICs is directly related to their enhanced capacity for fibroblast activation.

(F and G) Schematic showing a collective cell challenge for primary tumor growth into mammary fat pads (F) or a single-cell challenge for lung metastasis via the tail vein (G).

(H) Box plot showing the primary tumor burden in grams generated by the indicated sorted cells after overnight culture. Shown are data from three experiments using the indicated cell numbers (n = 4/group). IV, intravenous.

(I) Box plot showing the lung metastatic burden 5 weeks after tail vein injection. Two independent experiments are shown (n = 5–6/group). Shown are representative images of lungs with GFP^+ metastases.

Error bars represent SD in (C) and SEM in all other plots. *p < 0.05; ***p < 0.001; ****p < 0.0001; ns, not significant.

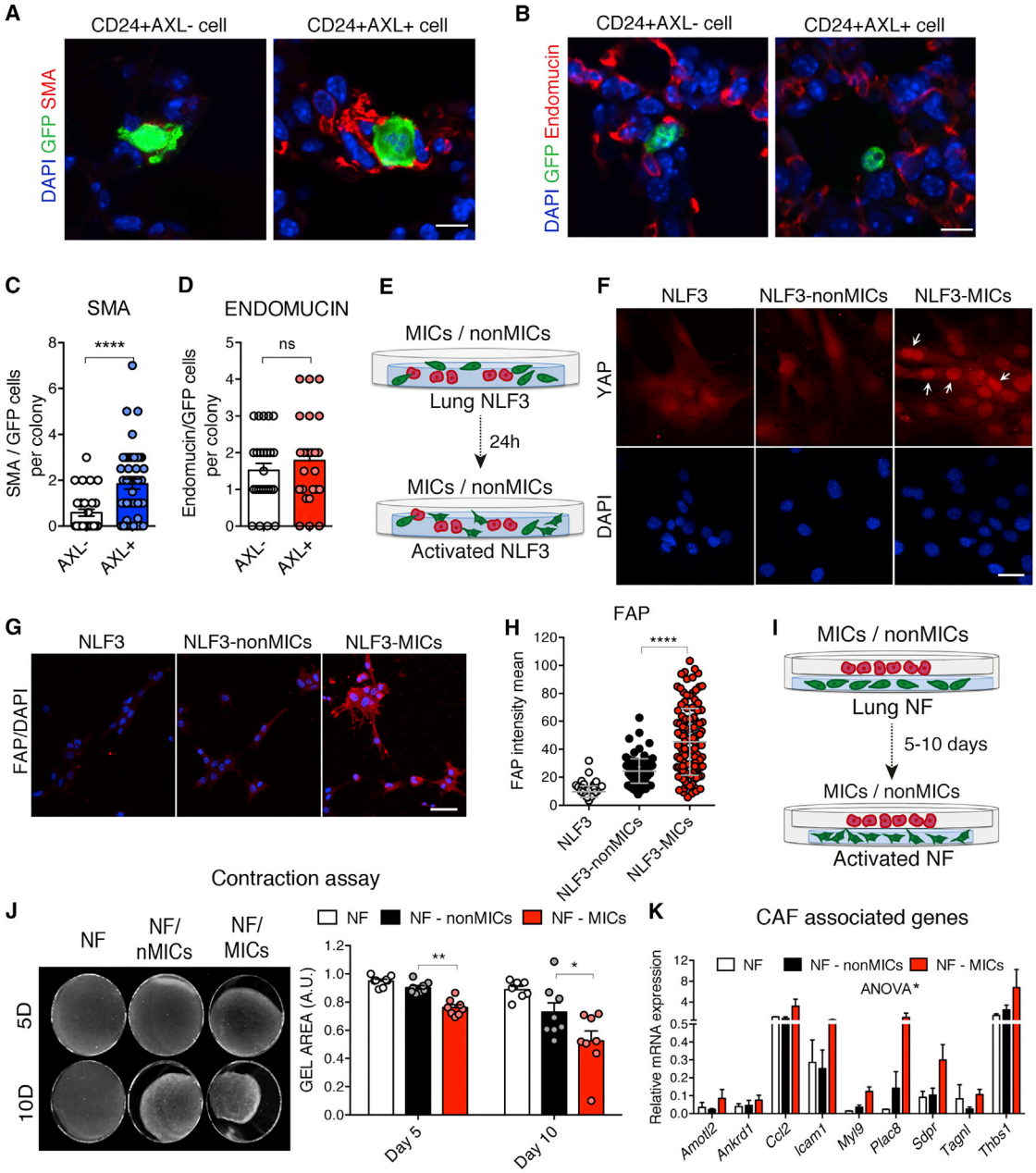

Figure 2. MICs Have a Higher Capacity to Activate Fibroblasts

(A–D) Representative pictures showing single GFP$^+$ cells (green) from the indicated subpools 72 hr after intravenous injection into RAG1-deficient mice. (A) DAPI staining (blue) and SMA (red); quantified in (C). (B) DAPI staining (blue) and Endomucin (red); quantified in (D). Scale bars, 10 μm. n = 32–50 cells.

(E) Schematic of the cancer cell and GFP$^+$ normal lung fibroblast cell line (NLF3) co-culture setting.

(F and G) Representative images of (F) early YAP nuclear translocation in NLF3 or (G) FAP levels in NLF3 cells 24 hr after plating. Scale bars, 40 μm (F), 70 μm (G).

(H) Chart indicating the levels of FAP in NLF3 cells from (G). Data are from one representative experiment of three.

(I) Schematic displaying the cancer cell and NLF3 co-culture setting.

(J) Representative images of the gel contraction by NLF3 assayed as in (I). The histogram shows the gel area of three independent experiments (n = 8/group).

(K) Quantitative real-time PCR analysis of the levels of CAF-defining genes in primary NF after co-culture with MICs (NF-MIC) or nonMICs (NF-nonMIC). Data are from at least three experiments in triplicate normalized to *Gapdh*. p = 0.0235 by ANOVA comparing differences between the NF, NF-non-MIC, and NF-MIC gene signatures.

Error bars represent SD in (H) and SEM in all other plots. *p < 0.05, **p < 0.01, ****p < 0.0001. ns, non-significant.

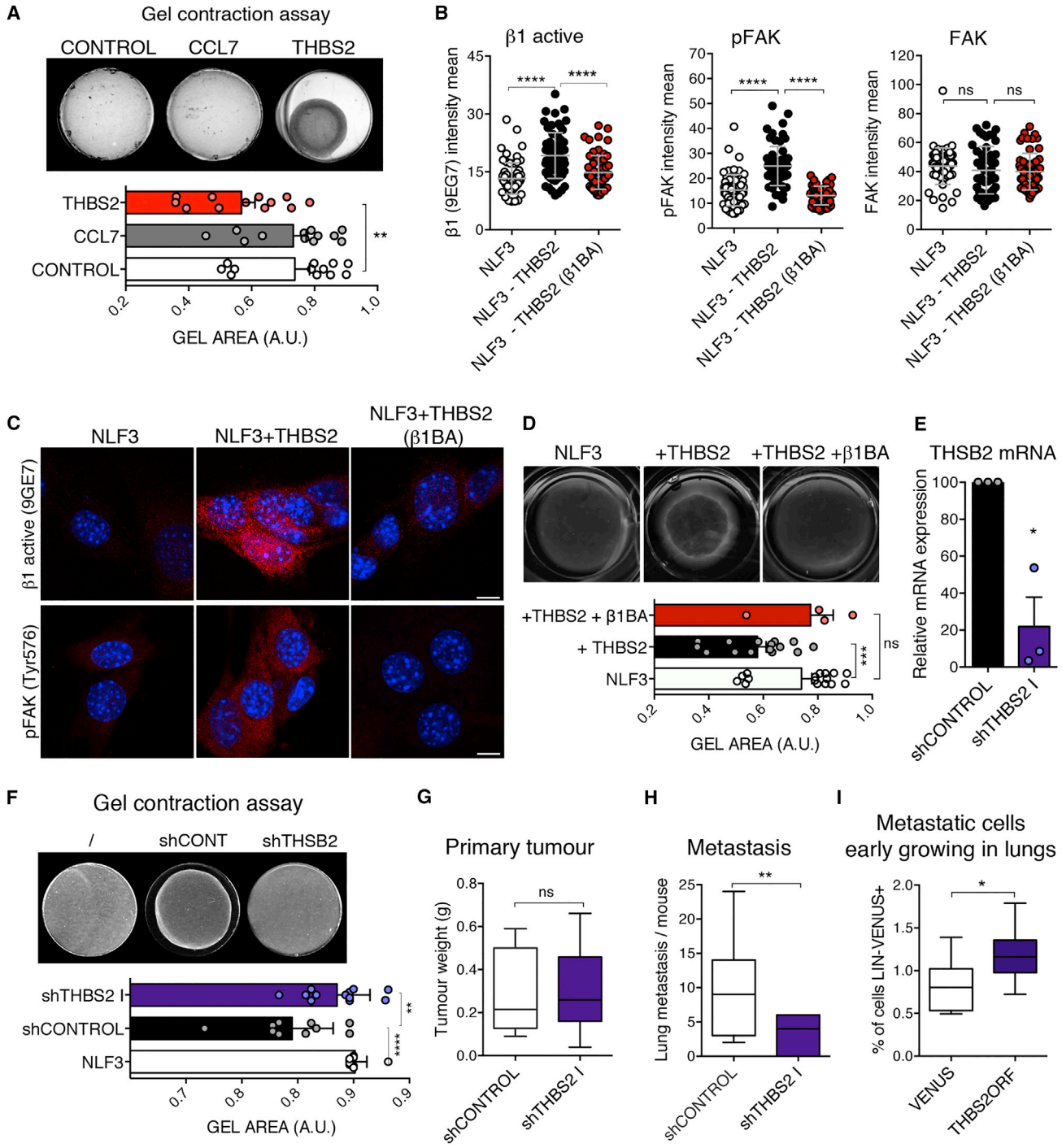

Figure 3. Cancer Cell-Derived THBS2 Enhances Fibroblast Activation

(A) Gel contraction induced by NLF3 after 3 days of exposure to recombinant CCL7 or THBS2. Top: representative NLF3-gels. Bottom: gel area quantification of three independent experiments (n = 12/group).

(B and C) Levels of the active isoform of integrin β1 (clone 9EG7) and its downstream effector FAK (total or phosphorylated) in NLF3 for the indicated groups. Data are from one representative experiment of two. Quantification is shown in (B) and representative images in (C). Scale bars, 20 μm.

(D) Gel contraction induced by NLF3 after co-culture with recombinant THBS2 with or without integrin β1-blocking antibody. Top: representative NLF3-gels. Bottom: gel area quantification of two independent experiments (n = 4–16/group).

(E) Quantitative real-time PCR analysis of the mRNA expression level of *Thbs2* by the indicated cells. Data are from three different experiments in triplicate normalized to Gapdh.

(legend continued on next page)

Cancer Cells Require AXL Mesenchymal Features to Facilitate Fibroblast Activation

We showed that MICs isolated from primary tumors are in an AXL-positive mesenchymal state. Therefore, we went on to examine the mesenchymal status of cancer cells at the target site by monitoring AXL expression during early colonization. We detected two distinct phases of AXL expression: a first phase, where the PyMT EMT MIC subpool maintains AXL, and a second phase, where the AXL-positive phenotype is lost coincidentally with MIC expansion in the lungs (Figure 5A). Similar biphasic AXL expression was observed in the MDA231 cell line (Figure 5B). Because the ability of cancer cells to trigger the niche is crucial for metastatic establishment (Figure 3) and dependent on the mesenchymal phenotype (Figure 4), we assessed whether the maintenance of AXL is required for the first phase of metastatic colonization. To do this, we inhibited AXL activity only during the first colonization phase by pre-treating cancer cells with the R428 inhibitor prior to intravenous injection and continued treatment in vivo for 7 days (Figure 5C and S5B). Notably, although R428 pre-treatment did not alter cancer cell extravasation (Figure S5C), it did significantly reduce metastasis after 5 weeks (Figures 5D–5F). Remarkably, only R428 pre-treatment 24 hr before seeding into the lung was sufficient to inhibit metastatic establishment (Figure 5E), suggesting that AXL mesenchymal features are required early after metastatic cell arrival to new tissue. Although short-term inhibition of AXL decreased metastatic competence, this had no effect on proliferation, self-renewal, and 3D cancer cell mass growth in vitro (Figures S5D–5G), or primary tumor initiation in vivo (Figure S5H). Interestingly, enhancing THBS2 expression in the MDA-MB-231 cell line partially rescued metastasis upon AXL inhibition in spite of the fact that THBS2 overexpression only provided a positive trend toward metastasis in these cells (Figures 5G, S5I, and S5J). This result is in line with the observation that AXL-mesenchymal cells show a THBS2-mediated advantage in niche activation. We also observed a block in metastasis upon AXL inhibition using shRNA knockdown in PyMT cells (Figures 5H and 5I). Furthermore, treatment of a second mouse breast cancer cell line (4T1) with shTHBS2 or shAXL also reduced the metastatic ability of 4T1 cells (Figures S5K and S5L). Together, these results suggest that the first phase of metastatic colonization requires the niche activation capacity provided by the AXL mesenchymal characteristics.

Activated Stroma Modulates the EMT of Cancer Cells toward a More Epithelial State

The previous results highlight the requirement of a mesenchymal state for metastatic initiation upon seeding at the target site. However, when cancer cells start growing within the metastatic tissue, AXL expression is downregulated (Figures 5A, 5B, and 6A). ImageStream analysis showed that, coincident with AXL downregulation, GFP^+ cancer cells growing in the lungs exhibit reduced expression of the EMT transcription factor Twist1 (Figures 6B, 6C, S6A, and S6B). This suggests that the previously reported EMT inhibition at the secondary site (Tsai et al., 2012) is controlled temporally within the second phase of metastatic colonization. Therefore, we investigated the changes that occur in metastatic cells during this time period.

Ex vivo co-culture (as shown in Figure 2E) demonstrated that, concomitant with fibroblast activation (Figures 2F–2H), MICs express lower levels of *Axl*, *Twist1* (Figures 6D and 6E), and overall EMT TF mRNA (Figure S6C). To track the phenotypic changes during this time, cancer cells were co-cultured with CAFs for 24 hr under adherence conditions (Figure S6D). Here we found that MICs reduced expression of Vimentin and AXL and increased expression of E-cadherin (Figures S6E and S6F). These results suggest that crosstalk between fibroblasts and cancer cells triggers alterations in both compartments; namely, activation of fibroblasts and consequent reacquisition of epithelial characteristics by cancer cells. To functionally validate these changes in the MIC EMT state, we analyzed their 3D invasion modality as they first come in contact with CAFs. In line with previous studies (Gaggioli et al., 2007; Yu et al., 2014), carcinoma cells in a non-invasive epithelial state (non-MICs) activated both single and collective cell invasion modalities. Strikingly, in line with the downregulation of mesenchymal markers, MICs displayed a notable reduction in single-cell migration when surrounded by CAFs (Figures 6F and 6G).

We next investigated the potential molecular mechanism of CAF-driven changes in cancer cells. TGF-β signaling has been implicated extensively in metastasis (Padua et al., 2008). High TGF-β signaling favors early metastatic colonization, whereas its subsequent reduction is important for metastatic outgrowth (Giampieri et al., 2009). Because TGF-β signaling, which is active in MICs (Figure 1A and S1B), could be linked functionally to their mesenchymal status (Diepenbruck et al., 2014), we assessed whether modulation of TGF-β signaling in MICs associates with the reacquisition of more epithelial characteristics. Using ImageStream analysis, we monitored the dynamics of activation of the TGF-β effector SMAD2-3 in metastasizing cells in vivo. As AXL^+ mesenchymal cells in the lung transit from the first to the second phase of colonization, the number and staining intensity of $pSMAD2\text{-}3^+$ cells decreased similarly to Twist1 expression (Figure 6H, S6G, and S6I). These data are in agreement with the previous evidence showing that a reduction in TGF-β signaling is required for the acquisition of the proliferative status necessary for metastatic outgrowth (Massagué, 2008). Conversely, the activation levels of BMP-dependent pSMAD1-5 was maintained during the second phase of colonization, and the number of $pSMAD1\text{-}5^+$ cells increased (Figures 6I, S6H, and S6J). In line

(F) Gel contraction induced by NLF3 after co-culture with the indicated cancer cells. Top: representative NLF3-gels. Bottom: gel area quantification of two independent experiments (n = 10–12/group).
(G) Box plot showing early primary tumor growth of primary PyMT cells expressing shCONTROL or shTHBS2 constructs in an orthotopic challenge (n = 6/group).
(H) Box plot showing the metastatic burden from PyMT cells expressing shCONTROL or shTHBS2 constructs 5 weeks after tail vein injection (n = 7–11/group). The superficial lung metastasis number was evaluated.
(I) Box plot displaying the metastatic cell content by flow cytometry 20 days after tail vein injection of PyMT control or THBS2ORF-expressing cells (n = 8/group).
Error bars represent SD in (B) and SEM in all other plots. *$p < 0.05$, **$p < 0.01$, ***$p < 0.001$, ****$p < 0.0001$.

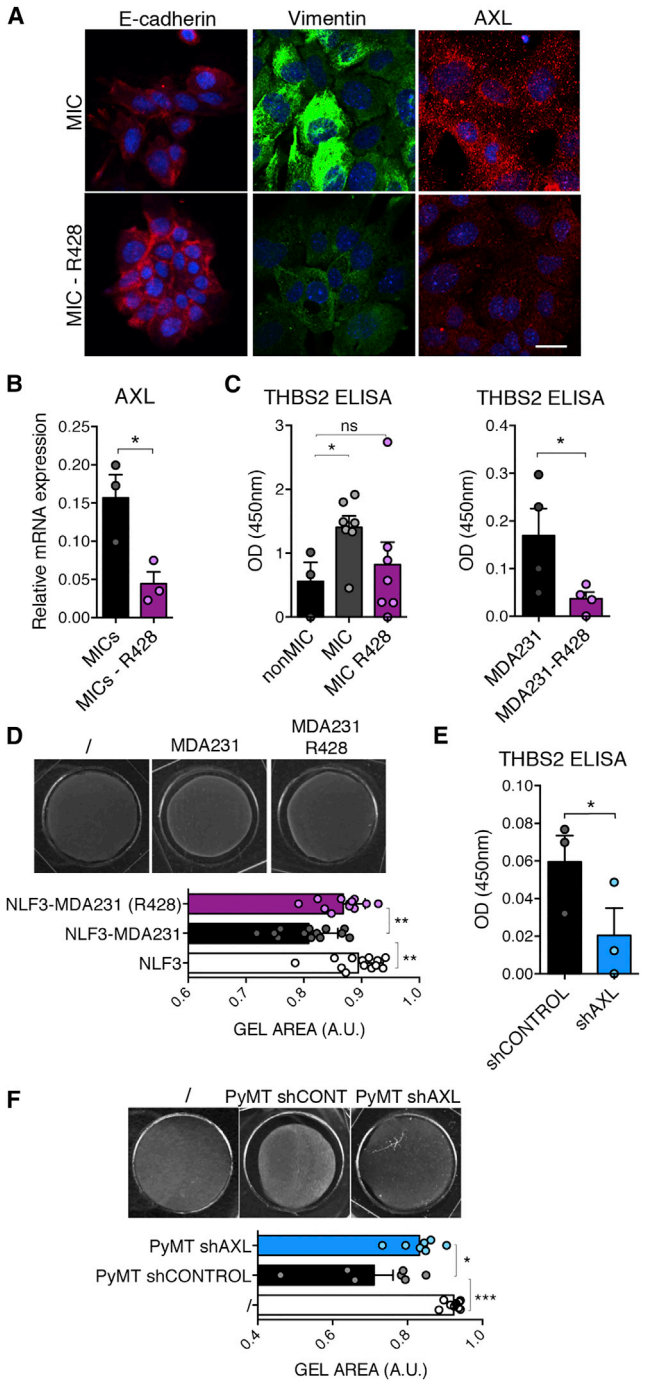

Figure 4. The Mesenchymal Status of Cancer Cells Drives Fibroblast Activation

(A) Representative images showing the expression of E-cadherin, Vimentin, and AXL in MICs 24 hr after treatment with DMSO or R428. Scale bar, 20 μm. See also Figure S4A.

(B) *Axl* gene expression levels in PyMT cells pre-treated with or without R428 as determined by quantitative real-time PCR analysis. Data are from three different experiments in triplicate (normalized to *Gapdh*).

(C) THBS2 secretion in the media collected from the indicated cancer cells 24 hr after R428 pre-treatment as measured by ELISA. Left: PyMT subpools, non-MIC data from three experiments in duplicate; MIC ± R428 treatment, data from seven experiments in duplicate. Right: MDA-MB-231 cell line (MDA231), data from four experiments in duplicate.

(D) Gel contraction induced by NLF3 after exposure to MDA231 pre-treated with DMSO or R428. Top: representative NLF3 gels. Bottom: gel area quantification of three independent experiments (n = 12/group).

(E) THBS2 secretion in the media collected from the indicated cancer cells 24 hr after plating by ELISA. Data are from three different experiments in duplicate.

(F) Gel contraction induced by NLF3 after exposure to the indicated cells. Top: representative NLF3 gels. Bottom: gel area quantification of two independent experiments (n = 7–9/group).

Error bars represent SEM. *$p < 0.05$, **$p < 0.01$, ***$p < 0.001$. ns, non-significant.

with this, we observed that the levels of inhibitor of differentiation 1 (ID1), a BMP/pSMAD1-5 target gene needed for cell proliferation during metastatic outgrowth (Gupta et al., 2007), were maintained, in particular in Twist1^{-} cells (Figures 6J and 6K). Notably, this modulation of ID1 in cancer cells could be recapitulated in vitro by exposure to CAF-conditioned medium (CaCM), which increases the levels of ID1 in a BMP-dependent manner (Figures 6L and 6M). Importantly, treatment with the specific inhibitor LDN193189 in vivo resulted in reduced metastatic capacity (Figures 6N and 6O), suggesting that BMP/pSMAD1-5 activity does indeed play a significant role in the second phase of colonization.

Together, these data show that, in the second colonization phase, the phenotypic changes observed in metastasizing cancer cells toward a more epithelial state correlate with an inhibition of TGF-β signaling and the enhanced BMP signaling necessary for metastatic outgrowth.

The Second Metastatic Colonization Phase Requires Temporal Regulation for Efficient Metastatic Establishment

We showed that the mesenchymal status of cancer cells during the first phase of colonization is required for metastatic establishment. However, when CD24^{+}AXL^{+} mesenchymal cancer cells accumulate in the lung, they revert to an AXL-negative, more epithelial state (Figure 5) following interaction with newly activated fibroblasts (Figure 6). If these two events were linked causally, then it would be expected that a temporal regulation of epithelial plasticity is critical for metastatic outgrowth. Initially, to probe this hypothesis, we induced an early mesenchymal reversion of metastatic cells by R428 treatment during the second phase of colonization (Figure 7A). This AXL inhibition no longer blocks the metastatic establishment of MDA231 cells (Figure S7A) and increases metastasis of primary PyMT cells (Figures 7B and 7C), suggesting that inhibiting EMT in this phase promotes metastasis. We observed that AXL inhibition in late-stage metastases did not alter the number of metastatic nodules (Figures 7A and 7B). Next, we delayed mesenchymal reversion in vivo by exogenous expression of the *Axl* gene (LTR-AXL) in cancer cells (Figure 7D). This leads to an exacerbated AXL-positive mesenchymal phenotype (Figures 7G, 7J, and S7B) without altering the proliferation capacity (Figure S7C). Importantly, preventing early AXL downregulation in metastasizing LTR-AXL-expressing cells delayed initial growth in the lungs (Figures 7E and 7F) and, ultimately, led to a reduction in the metastatic potential of both PyMT and MDA231 cancer cells (Figures 7H, 7I, and 7K). These data support the idea that downregulation of AXL is

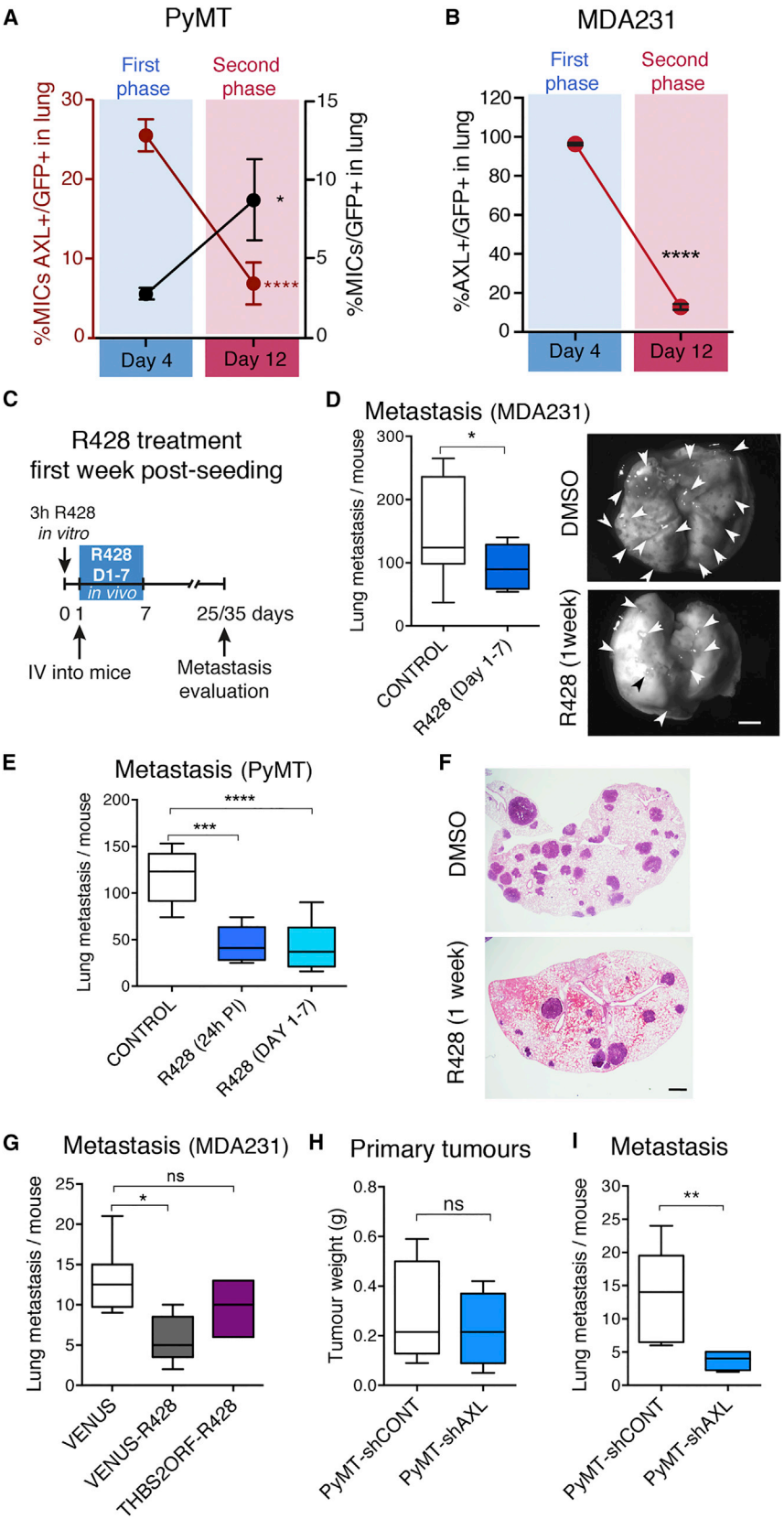

Figure 5. The Mesenchymal Status Is Regulated Temporally during Metastatic Colonization

(A) Flow cytometry analysis of the percentage of AXL$^+$ MICs (red, left y axis) and total MICs (black, right y axis) among total GFP$^+$ cancer cells in the lung 4 and 12 days after tail vein injection (n = 8–9/group from two independent experiments).

(B) Flow cytometry analysis of the percentage of AXL$^+$GFP$^+$ MDA-MB-231 cells (MDA231) among total GFP$^+$ cancer cells in the lung 4 and 12 days after tail vein injection (n = 3/group).

(C) Schematic of the R428 treatment setting for PyMT or MDA231 cells. IV, intravenous.

(D) Box plot showing the metastatic burden of MDA231 cells exposed to DMSO (n = 13) or R428 (n = 8) during the first week of colonization. The superficial lung metastasis number was evaluated. Shown are representative pictures of metastatic lungs. Scale bar, 300 μm.

(E) Box plot displaying the metastatic burden of PyMT cells pre-treated with DMSO (n = 14) or R428 (n = 5). In the last group (light blue, n = 9) mice were additionally treated with R428 during the first week of colonization. The superficial lung metastasis number was evaluated.

(F) Representative H&E staining of metastatic lung sections from the indicated mice. Scale bar, 100 μm.

(G) Box plot showing the metastatic burden of control (Venus) or THBS2-expressing MDA231 cells treated as in (C) (n = 7–5/group). Micrometastases were evaluated in histological sections of one lung lobe (see also Figure S5J).

(H) Box plot displaying early primary tumor growth after orthotopic transplantation of the indicated primary PyMT cells (n = 6/group).

(I) Box plot showing the metastatic burden of the indicated PyMT cells after tail vein injection (n = 5–8/group). The superficial lung metastasis number was evaluated.

Error bars represent SEM. *p < 0.05, **p < 0.01, ****p < 0.0001. ns, non-significant.

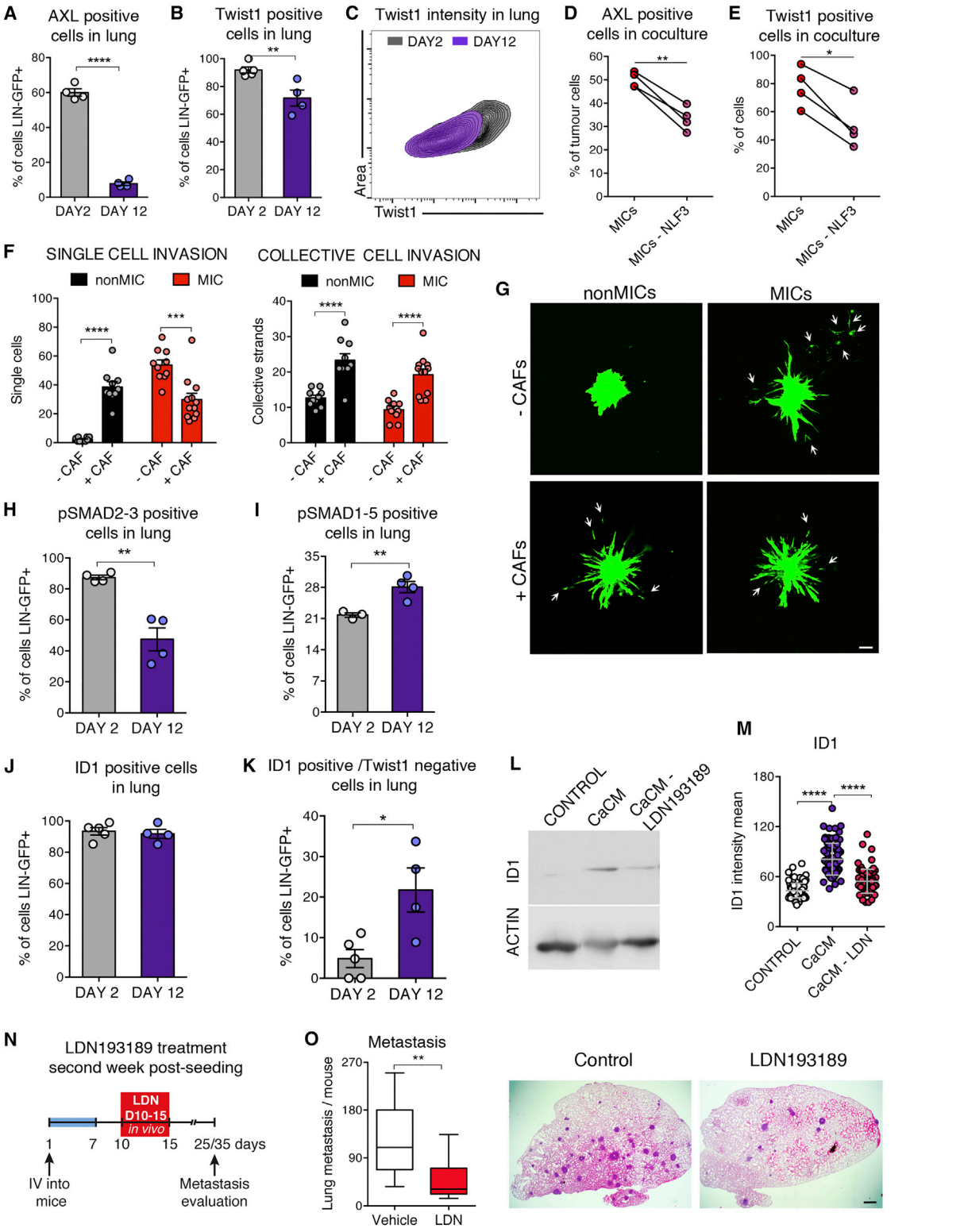

Figure 6. Attenuation of the Metastatic Cell Mesenchymal Phenotype

(A) Flow cytometry analysis changes in AXL$^+$ cancer cells seeded in the lungs after the indicated times points (n = 8–9/group). Data are from one representative experiment of two.

(legend continued on next page)

required during the second colonization phase to allow the transition to a more epithelial proliferative state. Interestingly, the overexpression of AXL in cancer cells led to a reduction in metastatic capacity specifically because an enhancement of primary tumor growth was detected (Figure S7D). This is likely due to an increase in AXL tyrosine kinase receptor activity at the early stages of tumor initiation, leading to the generation of larger tumors without obvious histologic changes after tumor establishment (Figures S7E and S7F).

DISCUSSION

Successful establishment of metastases requires cancer cells with self-renewal properties to disseminate from their tissue of origin and re-initiate growth at secondary sites. The evidence that experimental induction of EMT in epithelial cells triggers stem cell characteristics suggests a unified mechanism for cancer metastasis. However, the plasticity of the EMT program from dissemination to distant colonization during the metastatic process makes the direct relationship between EMT and stemness controversial (Tsai et al., 2012; Mani et al., 2008; Morel et al., 2008; Wellner et al., 2009; Brabletz, 2012; Nieto, 2013) and suggests that metastatic cancer cells are likely to undergo a partial EMT that can be modulated toward a more mesenchymal or epithelial state (Ombrato and Malanchi, 2014). Furthermore, although the requirement of an EMT inhibition at the metastatic site has been reported previously (Tsai et al., 2012), the dynamic regulation of the mesenchymal/epithelial transition is currently unknown. Using breast cancer models, we highlight the importance of the more mesenchymal phenotype of MICs during the early phase of metastatic colonization. Moreover, we demonstrate the requirement for AXL mesenchymal state-dependent THBS2 secretion in mediating enhanced niche activation. We also identify a subsequent phase of colonization where the mesenchymal phenotype of cancer cells is downmodulated by the interaction with the newly induced niche. This crosstalk leads to inhibition of TGF-β signaling and pSMAD1-5-dependent outgrowth, shifting cancer cells toward a more epithelial and proliferative state. Blocking the effectors of these pathways during this biphasic process reduces metastasis: THBS2 expression during the first phase or pSMAD1-5 activity during the second phase. Here we identify epithelial plasticity as a crucial determinant of metastatic colonization and describe how disruption of AXL-dependent phenotypic modulation is sufficient to reduce metastatic efficiency.

In agreement with the previously observed link between the EMT program and the gain in stemness (Mani et al., 2008; Morel et al., 2008), we found that the MICs of the MMTV-PyMT tumor model (Malanchi et al., 2012) display a mesenchymal phenotype (Figure 1A–1D and S1). However, using the EMT downstream effector AXL as a marker for mesenchymal cancer cells, we demonstrate that, within the MMTV-PyMT hierarchy, the mesenchymal features per se do not confer a differential tumor initiation ability (Figure 1H and S2). Nonetheless, a more mesenchymal state promotes growth at a less favorable distant environment (Figure 1I). This correlates with a higher capacity of $CD24^+AXL^+$ cells to induce stromal activation early after infiltration of the secondary tissue (Figures 2A–2D). Our work suggests that the increased intrinsic ability to trigger a favorable microenvironment at the naive target site provides a metastatic initiation advantage. Indeed, both the MIC subpool of MMTV-PyMT cancer cells as well as the metastatic human MDA-MB-231 cell line show higher niche component activation ability according to their mesenchymal phenotype (Figures 2 and 4) and THBS2 secretion (Figure 3). We show here that THBS2 is capable of triggering fibroblast activation via integrin signaling and enhancing early metastatic colonization (Figure 3I). This finding is supported by computational analyses defining *Thbs2* as one of the three genes associated with a stromal desmoplastic reaction and high metastatic risk (Kim et al., 2010) as well as by the clinical evidence of its correlation with poor prognosis in high-grade human breast cancers (Figure S3I). However, in rare circulating cancer cell clusters that exhibit high metastatic potential, the mechanism we describe may be circumvented (Aceto et al., 2014). In this context, the cells within the cluster may create their own favorable niche and, therefore, bypass the requirement for a mesenchymal state and associated niche activation.

Our results support the concept that stemness is unperturbed by the mesenchymal/epithelial plasticity of metastatic cells and correlate with a flexible partial EMT state rather than with a stable binary EMT program. We confirmed that, to efficiently generate a cancer cell mass at a distant site, cells regain a more epithelial phenotype (Tsai et al., 2012). Notably, we now show that this modulation is controlled temporally during the second phase of metastatic

(B and C) ImageStream analysis changes in Twist1 expression in AXL^+ cancer cells seeded in the lungs after the indicated times points (n = 4–5/group). (B) Quantification of $Twist1^+$ cells from one representative experiment of three. (C) Contour plot of representative lungs from (B) showing Twist1 staining intensity. (D and E) MIC changes after 3–5 days of co-culture with NLF3 as in Figure 2E. (D) Flow cytometry quantification of AXL expression levels. Data are from one representative experiment (n = 4/group) of two. (E) ImageStream analysis of the percentage of $Twist1^+$ cells. Data are from one representative experiment (n = 4/group) of two.

(F and G) Spheroid invasion assay. Labeled MIC or non-MIC (green) spheroids were imaged 48 hr after seeding into Matrigel:collagen I with or without CAFs. (F) Quantification of single (left) and collective (right) cell invasion. Data are from one representative experiment of two. (G) Representative spheroid images. Arrows indicate single invading cells. Scale bar, 100 μm.

(H–K) ImageStream analysis of $pSMAD2\text{-}3^+$ (H), $pSMAD1\text{-}5^+$ (I), $ID1^+$ (J), and $ID1^+Twist1^-$ (K) cell percentages in the lung 2 or 12 days post-seeding (n = 3–5/group).

(L and M) Expression levels of ID1 in primary $CD24^+AXL^+$ tumor cells 24 hr after exposure to the indicated media and in the presence of LDN193189 inhibitor determined by (L) western blot using Actin as a loading control (one representative experiment of two) or (M) immunofluorescence staining quantification (one representative experiment of two).

(N) Schematic showing the in vivo LDN193189 treatment setting.

(O) Box plot displaying the metastatic burden of PyMT cells in mice treated with vehicle or LDN193189. Shown are representative H&E-stained lung sections (n = 9–12/group). Scale bar, 100 μm.

Error bars represent SD in (M) and SEM in all other plots. *$p < 0.05$, **$p < 0.01$, ***$p<0.001$, ****$p < 0.0001$. ns, non-significant.

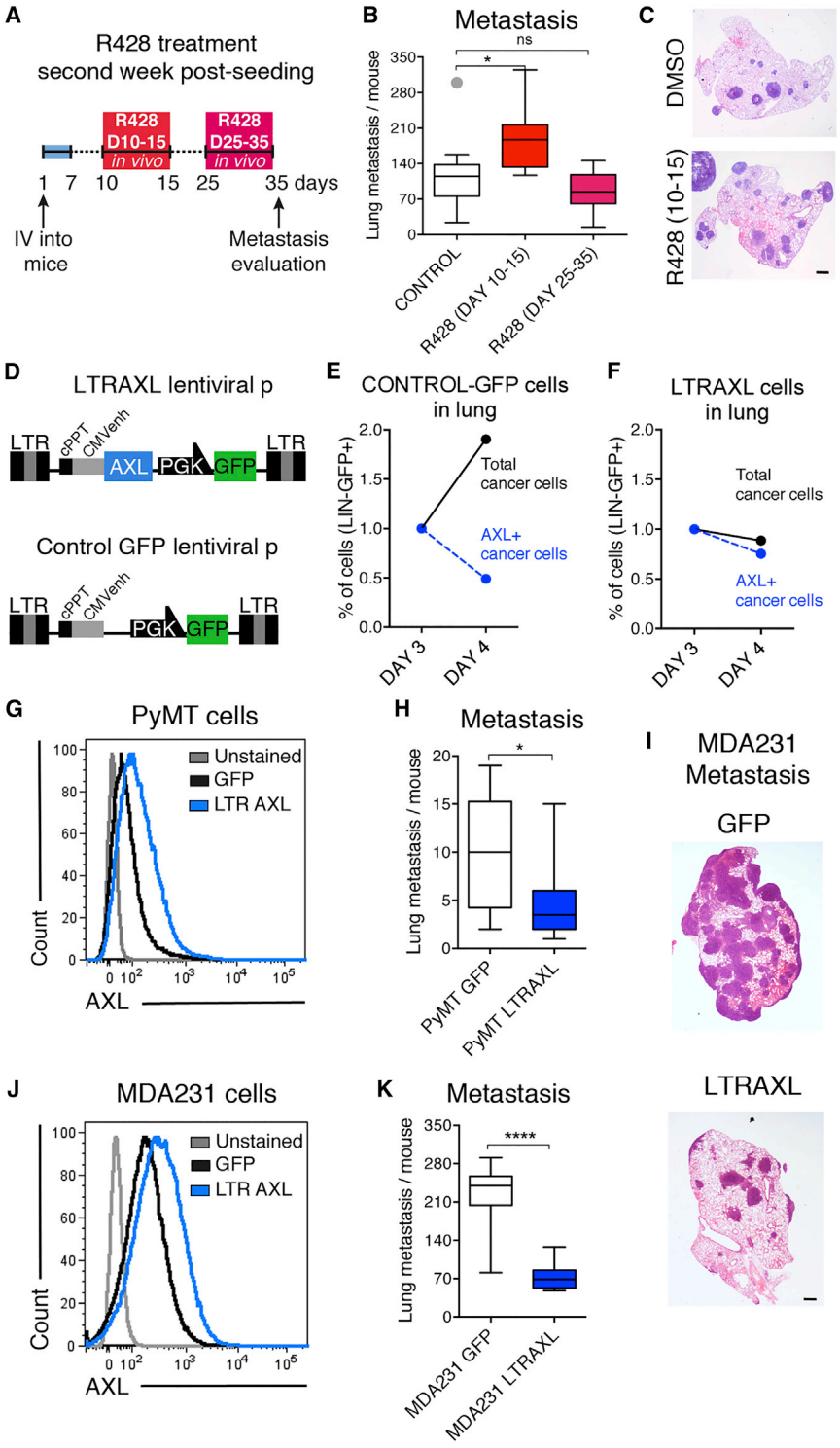

Figure 7. EMT-Stabilized Cells Do Not Metastasize Efficiently

(A) Schematic showing the R428 treatment setting.

(B) Box plot displaying the metastatic burden of mice injected with primary PyMT cells for the indicated groups: DMSO, n = 11; R428, days 10–15, n = 10; and R428, days 25–35, n = 7. The superficial lung metastasis number was evaluated.

(C) Representative images of the indicated lung sections. Scale bar, 100 μm.

(D) Schematic of the LTR-driven lentiviral plasmid expressing the human *Axl* open reading frame (ORF) (top) and control plasmid (bottom).

(E and F) Flow cytometry analysis showing the percentage of total cancer cells (black) and AXL$^+$ cells (blue) in the lung 3 or 4 days after intravenous injection of MDA231 expressing the control-GFP construct (E) or LTR-AXL construct (F). Data are displayed as the group average relative to day 3 (n = 4–6/group).

(G) Representative flow cytometry plot showing the expression levels of AXL in the indicated primary PyMT cells.

(H) Box plot showing superficial lung metastasis quantification after intravenous injection of PyMT cells expressing control-GFP or LTR-AXL constructs (n = 10/group).

(I) Representative H&E staining of lung sections of mice injected with MDA231 of the indicated groups. Scale bar, 100 μm.

(J) Representative flow cytometry plot showing the expression levels of AXL in the indicated MDA231 cells.

(K) Box plot showing the superficial metastasis quantification after intravenous injection of MDA231 cells expressing the control-GFP or LTR-AXL constructs (n = 8/group).

Error bars represent SEM. *p < 0.05, ****p < 0.0001.

colonization (Figure 7). Indeed, prolonged *Axl* gene activation in cancer cells strongly reduces metastatic ability (Figures 7H and 7K). AXL expression in the context of breast cancer lung metastasis opposes primary tumor initiation (Figures 7G–7K and S7D), likely because of differences in the requirement of its tyrosine kinase receptor function, which is also crucial for other cancer types (Ben-Batalla et al., 2013).

Remarkably, we provide experimental evidence that epithelial plasticity is mediated by crosstalk between the cancer cell and stroma (Figure 6). During the second colonization phase, the newly activated fibroblasts generated during the first phase induce a phenotype switch in MICs. BMP-dependent ID1 activation in cancer cells is triggered by exposure to CaCM (Figures 6L and 6M). This effect, observed in vitro, is corroborated in vivo by the enhancement of pSMAD1-5 activity and downmodulation of TGF-β signaling in favor of an ID1-positive proliferative state. Indeed, treatment of mice with the specific BMP inhibitor LDN193189 during the second colonization phase inhibits metastasis (Figures 6N and 6O).

Overall, this study provides a refined definition of distant colonization by more mesenchymal cancer cells where their

niche-activation capacity is linked to their mesenchymal status and THBS2 secretion. Subsequently, activated fibroblasts drive MICs to revert to a more epithelial phenotype. This model highlights the importance of cancer cell-stroma crosstalk in modulating the optimal phenotype for cancer cells during the dynamic metastatic process.

EXPERIMENTAL PROCEDURES

Statistical Analysis

Statistical analyses were performed using Prism software (GraphPad Software). p values were obtained from two-tailed Student's t tests with paired or unpaired adjustment. One-column t test was used for comparisons with a normalized value. One-tailed t test was used for Figure 4E. Where indicated, two-way ANOVA was used to perform multiple comparisons or multiple variables analysis between experimental groups. Significance was set at $p < 0.05$. Graphs show the symbols describing the p value (*$p < 0.05$, **$p < 0.01$, ***$p < 0.001$, ****$p < 0.0001$).

Animal Procedures

All experimental procedures involving mice were performed in accordance with United Kingdom regulations under project license PPL 80/2531. Further information can be found in the Supplemental Experimental Procedures.

ImageStream Analysis

Lungs or Matrigel collagen gels from co-culture experiments were digested and dissociated to obtain a single-cell suspension, stained with a live/dead fixable dye, fixed, and stained with the indicated primary antibodies (antibody descriptions and working dilutions can be found in Table S4 and in the Supplemental Experimental Procedures). Tumor cells in the lung were identified by GFP expression. The acquired ImageStream data were analyzed using Amnis IDEA management software.

ACCESSION NUMBERS

The accession number for the microarray data reported in this paper is GEO: GSE63558.

SUPPLEMENTAL INFORMATION

Supplemental Information includes Supplemental Experimental Procedures, seven figures, and four tables and can be found with this article online at http://dx.doi.org/10.1016/j.celrep.2015.11.025.

AUTHOR CONTRIBUTIONS

Y.P.M. designed and performed most of the experiments, analyzed data, and contributed to manuscript preparation. D.P. designed and performed the invasion experiments and analyzed data. A.R performed pSMAD1-5 and ID1 detection in vitro and analyzed data. L.O. and F.C. performed pilot experiments and contributed to discussions. P.C. performed the bioinformatics analysis. B.S.D. performed staining of the lung sections. S.D. provided critical reagents. C.H. and E.S. designed and supervised some experiments, provided crucial conceptual advice, and revised the manuscript. I.M. designed and supervised the study, interpreted data, and wrote the manuscript.

ACKNOWLEDGMENTS

We thank the members of the Tumour Host Interaction Laboratory (THI) and Tumour Cell Biology Lab (TCB) at the Crick Institute for support and discussions. Particularly, we thank Dr. Laurie Gay, Stefanie Wculek (THI), and Dr. Marco Montagner (TCB) for critically reading the manuscript. We are thankful to Robert Moore from the THI, Emma Nye from the Experimental Histopathology unit, Julie Bee from the Biological Resources unit, and all members of the FACS laboratory at Crick Institute for invaluable technical help. We thank Dr. Levi A. Garraway from the Broad Institute of Harvard and Dr. Paul Bornstein from the Biochemistry and Medicine Department, University of Washington, for sharing, through Addgene, the pDONR223-AXL and pcDNA3-mTHBS2 plasmids, respectively.

Received: November 28, 2014
Revised: October 5, 2015
Accepted: November 4, 2015
Published: December 3, 2015

REFERENCES

Aceto, N., Bardia, A., Miyamoto, D.T., Donaldson, M.C., Wittner, B.S., Spencer, J.A., Yu, M., Pely, A., Engstrom, A., Zhu, H., et al. (2014). Circulating tumor cell clusters are oligoclonal precursors of breast cancer metastasis. Cell *158*, 1110–1122.

Ben-Batalla, I., Schultze, A., Wroblewski, M., Erdmann, R., Heuser, M., Waizenegger, J.S., Riecken, K., Binder, M., Schewe, D., Sawall, S., et al. (2013). Axl, a prognostic and therapeutic target in acute myeloid leukemia mediates paracrine crosstalk of leukemia cells with bone marrow stroma. Blood *122*, 2443–2452.

Brabletz, T. (2012). EMT and MET in metastasis: where are the cancer stem cells? Cancer Cell *22*, 699–701.

Calvo, F., Ege, N., Grande-Garcia, A., Hooper, S., Jenkins, R.P., Chaudhry, S.I., Harrington, K., Williamson, P., Moeendarbary, E., Charras, G., and Sahai, E. (2013). Mechanotransduction and YAP-dependent matrix remodelling is required for the generation and maintenance of cancer-associated fibroblasts. Nat. Cell Biol. *15*, 637–646.

Chen, J., Li, Y., Yu, T.-S., McKay, R.M., Burns, D.K., Kernie, S.G., and Parada, L.F. (2012). A restricted cell population propagates glioblastoma growth after chemotherapy. Nature *488*, 522–526.

Diepenbruck, M., Waldmeier, L., Ivanek, R., Berninger, P., Arnold, P., van Nimwegen, E., and Christofori, G. (2014). Tead2 expression levels control the subcellular distribution of Yap and Taz, zyxin expression and epithelial-mesenchymal transition. J. Cell Sci. *127*, 1523–1536.

Gaggioli, C., Hooper, S., Hidalgo-Carcedo, C., Grosse, R., Marshall, J.F., Harrington, K., and Sahai, E. (2007). Fibroblast-led collective invasion of carcinoma cells with differing roles for RhoGTPases in leading and following cells. Nat. Cell Biol. *9*, 1392–1400.

Giampieri, S., Manning, C., Hooper, S., Jones, L., Hill, C.S., and Sahai, E. (2009). Localized and reversible TGF-β signalling switches breast cancer cells from cohesive to single cell motility. Nat. Cell Biol. *11*, 1287–1296.

Gjerdrum, C., Tiron, C., Høiby, T., Stefansson, I., Haugen, H., Sandal, T., Collett, K., Li, S., McCormack, E., Gjertsen, B.T., et al. (2010). Axl is an essential epithelial-to-mesenchymal transition-induced regulator of breast cancer metastasis and patient survival. Proc. Natl. Acad. Sci. USA *107*, 1124–1129.

Gupta, G.P., Perk, J., Acharyya, S., de Candia, P., Mittal, V., Todorova-Manova, K., Gerald, W.L., Brogi, E., Benezra, R., and Massagué, J. (2007). ID genes mediate tumor reinitiation during breast cancer lung metastasis. Proc. Natl. Acad. Sci. USA *104*, 19506–19511.

Hermann, P.C., Huber, S.L., Herrler, T., Aicher, A., Ellwart, J.W., Guba, M., Bruns, C.J., and Heeschen, C. (2007). Distinct populations of cancer stem cells determine tumor growth and metastatic activity in human pancreatic cancer. Cell Stem Cell *1*, 313–323.

Holland, S.J., Pan, A., Franci, C., Hu, Y., Chang, B., Li, W., Duan, M., Torneros, A., Yu, J., Heckrodt, T.J., et al. (2010). R428, a selective small molecule inhibitor of Axl kinase, blocks tumor spread and prolongs survival in models of metastatic breast cancer. Cancer Res. *70*, 1544–1554.

Kim, H., Watkinson, J., Varadan, V., and Anastassiou, D. (2010). Multi-cancer computational analysis reveals invasion-associated variant of desmoplastic reaction involving INHBA, THBS2 and COL11A1. BMC Med. Genomics *3*, 51.

Liu, J.C., Deng, T., Lehal, R.S., Kim, J., and Zacksenhaus, E. (2007). Identification of tumorsphere- and tumor-initiating cells in HER2/Neu-induced mammary tumors. Cancer Res. *67*, 8671–8681.

Malanchi, I. (2013). Tumour cells coerce host tissue to cancer spread. Bonekey Rep. *2*, 371.

Malanchi, I., Peinado, H., Kassen, D., Hussenet, T., Metzger, D., Chambon, P., Huber, M., Hohl, D., Cano, A., Birchmeier, W., and Huelsken, J. (2008). Cutaneous cancer stem cell maintenance is dependent on beta-catenin signalling. Nature *452*, 650–653.

Malanchi, I., Santamaria-Martínez, A., Susanto, E., Peng, H., Lehr, H.-A., Delaloye, J.-F., and Huelsken, J. (2012). Interactions between cancer stem cells and their niche govern metastatic colonization. Nature *481*, 85–89.

Mani, S.A., Guo, W., Liao, M.-J., Eaton, E.N., Ayyanan, A., Zhou, A.Y., Brooks, M., Reinhard, F., Zhang, C.C., Shipitsin, M., et al. (2008). The epithelial-mesenchymal transition generates cells with properties of stem cells. Cell *133*, 704–715.

Massagué, J. (2008). TGFbeta in Cancer. Cell *134*, 215–230.

Morel, A.-P., Lièvre, M., Thomas, C., Hinkal, G., Ansieau, S., and Puisieux, A. (2008). Generation of breast cancer stem cells through epithelial-mesenchymal transition. PLoS ONE *3*, e2888.

Nguyen, D.X., Chiang, A.C., Zhang, X.H.-F., Kim, J.Y., Kris, M.G., Ladanyi, M., Gerald, W.L., and Massagué, J. (2009). WNT/TCF signaling through LEF1 and HOXB9 mediates lung adenocarcinoma metastasis. Cell *138*, 51–62.

Nieto, M.A. (2013). Epithelial plasticity: a common theme in embryonic and cancer cells. Science *342*, 1234850.

Ombrato, L., and Malanchi, I. (2014). The EMT universe: space between cancer cell dissemination and metastasis initiation. Crit. Rev. Oncog. *19*, 349–361.

Oskarsson, T., Acharyya, S., Zhang, X.H.-F., Vanharanta, S., Tavazoie, S.F., Morris, P.G., Downey, R.J., Manova-Todorova, K., Brogi, E., and Massagué, J. (2011). Breast cancer cells produce tenascin C as a metastatic niche component to colonize the lungs. Nat. Med. *17*, 867–874.

Paccez, J.D., Vogelsang, M., Parker, M.I., and Zerbini, L.F. (2014). The receptor tyrosine kinase Axl in cancer: biological functions and therapeutic implications. Int. J. Cancer *134*, 1024–1033.

Padua, D., Zhang, X.H.-F., Wang, Q., Nadal, C., Gerald, W.L., Gomis, R.R., and Massagué, J. (2008). TGFbeta primes breast tumors for lung metastasis seeding through angiopoietin-like 4. Cell *133*, 66–77.

Peinado, H., Olmeda, D., and Cano, A. (2007). Snail, Zeb and bHLH factors in tumour progression: an alliance against the epithelial phenotype? Nat. Rev. Cancer *7*, 415–428.

Qian, B.-Z., Li, J., Zhang, H., Kitamura, T., Zhang, J., Campion, L.R., Kaiser, E.A., Snyder, L.A., and Pollard, J.W. (2011). CCL2 recruits inflammatory monocytes to facilitate breast-tumour metastasis. Nature *475*, 222–225.

Reya, T., and Clevers, H. (2005). Wnt signalling in stem cells and cancer. Nature *434*, 843–850.

Sheridan, C. (2013). First Axl inhibitor enters clinical trials. Nat. Biotechnol. *31*, 775–776.

Sleeman, J.P. (2012). The metastatic niche and stromal progression. Cancer Metastasis Rev. *31*, 429–440.

Thiery, J.P., Acloque, H., Huang, R.Y.J., and Nieto, M.A. (2009). Epithelial-mesenchymal transitions in development and disease. Cell *139*, 871–890.

Tichet, M., Prod'Homme, V., Fenouille, N., Ambrosetti, D., Mallavialle, A., Cerezo, M., Ohanna, M., Audebert, S., Rocchi, S., Giacchero, D., et al. (2015). Tumour-derived SPARC drives vascular permeability and extravasation through endothelial VCAM1 signalling to promote metastasis. Nat. Commun. *6*, 6993.

Tsai, J.H., Donaher, J.L., Murphy, D.A., Chau, S., and Yang, J. (2012). Spatiotemporal regulation of epithelial-mesenchymal transition is essential for squamous cell carcinoma metastasis. Cancer Cell *22*, 725–736.

Vermeulen, L., De Sousa E Melo, F., van der Heijden, M., Cameron, K., de Jong, J.H., Borovski, T., Tuynman, J.B., Todaro, M., Merz, C., Rodermond, H., et al. (2010). Wnt activity defines colon cancer stem cells and is regulated by the microenvironment. Nat. Cell Biol. *12*, 468–476.

Vuoriluoto, K., Haugen, H., Kiviluoto, S., Mpindi, J.-P., Nevo, J., Gjerdrum, C., Tiron, C., Lorens, J.B., and Ivaska, J. (2011). Vimentin regulates EMT induction by Slug and oncogenic H-Ras and migration by governing Axl expression in breast cancer. Oncogene *30*, 1436–1448.

Wellner, U., Schubert, J., Burk, U.C., Schmalhofer, O., Zhu, F., Sonntag, A., Waldvogel, B., Vannier, C., Darling, D., zur Hausen, A., et al. (2009). The EMT-activator ZEB1 promotes tumorigenicity by repressing stemness-inhibiting microRNAs. Nat. Cell Biol. *11*, 1487–1495.

Yu, Y., Xiao, C.-H., Tan, L.-D., Wang, Q.-S., Li, X.-Q., and Feng, Y.-M. (2014). Cancer-associated fibroblasts induce epithelial-mesenchymal transition of breast cancer cells through paracrine TGF-β signalling. Br. J. Cancer *110*, 724–732.